Title

Simultaneous imaging of 13C metabolism and 1H structure: technical considerations and potential applications.

Journal

NMR in Biomedicine, 28(5)

Authors

Gordon, Jeremy
Fain, Sean
Niles, David
et al.

Publication Date

2015-05-01

DOI

10.1002/nbm.3279

Peer reviewed

HHS Public Access

Author manuscript

NMR Biomed. Author manuscript; available in PMC 2016 May 01.

Published in final edited form as:

NMR Biomed. 2015 May ; 28(5): 576–582. doi:10.1002/nbm.3279.

Simultaneous Imaging of ^{13}C Metabolism and ^{1}H Structure: Technical Considerations and Potential Applications

Jeremy W. Gordon[1], **Sean B. Fain**[1,2,3,*], **David J. Niles**[1], **Kai D. Ludwig**[1], **Kevin M. Johnson**[1], and **Eric T. Peterson**[1]

[1]Department of Medical Physics, University of Wisconsin, Madison, Wisconsin, USA

[2]Department of Radiology, University of Wisconsin, Madison, Wisconsin, USA

[3]Department of Biomedical Engineering, University of Wisconsin, Madison, Wisconsin, USA

Abstract

Real-time imaging of ^{13}C metabolism in-vivo has been enabled by recent advances in hyperpolarization. Due to the inherently low natural abundance of endogenous ^{13}C nuclei, hyperpolarized ^{13}C images lack structural information that could be used to aid in motion detection and anatomic registration. Motion before or during the ^{13}C acquisition can therefore result in artifacts and misregistration that may obscure measures of metabolism. In this work, we demonstrate a method to simultaneously image both ^{1}H and ^{13}C nuclei using a dual-nucleus spectral-spatial RF excitation and a fully coincident readout for rapid multinuclear spectroscopic imaging. With the appropriate multinuclear hardware, and the means to simultaneously excite and receive on both channels, this technique is straightforward to implement and requires little-to-no increase in scan time. Phantom and in-vivo experiments were performed with both Cartesian and spiral trajectories to validate and illustrate the utility of simultaneous acquisitions. Motion compensation of dynamic metabolic measurements acquired during free breathing is demonstrated using motion tracking derived from ^{1}H data. Simultaneous multinuclear imaging provides structural ^{1}H and metabolic ^{13}C images that are correlated both spatially and temporally, and are therefore amenable to joint ^{1}H and ^{13}C analysis and correction of structure-function images.

Graphical Abstract

Simultaneous excitation of ^{1}H and hyperpolarized ^{13}C spins with spectral-spatial RF pulses enables near real-time multinuclear spectroscopic imaging. By virtue of the simultaneous excitation, structural ^{1}H and functional ^{13}C metabolite maps are both spatially and temporally correlated, thus mitigating artifacts and misregistration between the two datasets. With the appropriate multinuclear hardware this technique is easily implemented, compatible with any k-space trajectory, and results in little-to-no increase in scan time.

Corresponding Author: Sean B. Fain PhD, Department of Medical Physics, 1111 Highland Ave., 1133 Wisconsin Institutes for Medical Research, University of Wisconsin – Madison, Madison WI 53705.

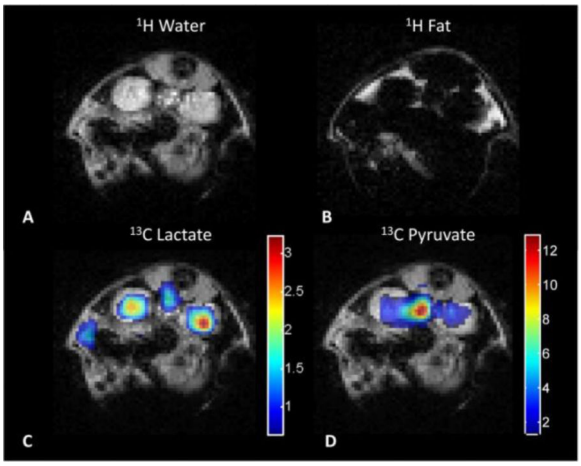

Keywords

DNP; hyperpolarized; spectral-spatial excitation; spiral; pyruvate; simultaneous

Introduction

Recent advances in hyperpolarized (HP) MRI techniques (1) have kindled renewed interest in direct imaging of non-proton nuclei with magnetic resonance. Near real-time imaging of ^{13}C nuclei is enabled by hyperpolarization, yielding a >10,000 increase in spin polarization compared to Boltzmann equilibrium. HP carbon agents have rapidly expanded from inert vascular agents (2, 3) to metabolic studies which primarily use [1-^{13}C]pyruvate (4–9). The [1-^{13}C]pyruvate metabolite is the major input to the citric acid cycle and sits at the nexus of metabolism. The rapid conversion of [1-^{13}C]pyruvate into [1-^{13}C]lactate has most commonly been used as a noninvasive biomarker of cancer (6, 10) but conversion into [1-^{13}C]alanine (11) or ^{13}C bicarbonate (12) is also readily observable in the timeframe of a hyperpolarized experiment. In addition, other ^{13}C labeled, metabolically active molecules (13–15) and other nuclei (16–19) have been successfully polarized and studied for measurement of pH and necrosis.

Unlike conventional ^{1}H MRI, hyperpolarized ^{13}C imaging studies have excellent contrast due to the lack of background signal from endogenous metabolites. Yet, structural information from ^{1}H anatomic images must be acquired to properly localize the metabolic data. Typically, the ^{1}H anatomic images are acquired before or after the ^{13}C acquisition, adding several seconds or minutes to the total scan time. As a result, motion before or during the ^{13}C acquisition can result in artifacts and misregistration relative to ^{1}H anatomic images that may obfuscate measures of metabolism. To reduce scan times and the potential for motion blurring and misregistration between thermally polarized ^{1}H and non-^{1}H datasets, several groups have reported simultaneous (20) and interleaved (21) spectroscopy, as well as simultaneous (22–24) and interleaved (25, 26) imaging of multiple nuclei.

However, imaging of HP ^{13}C nuclei places unique demands on the MR acquisition for both interleaved and simultaneous methods due to the need for rapid and RF efficient

spectroscopic imaging techniques (27, 28), with different spectral resolution and flip angle requirements for both nuclei. Interleaved and sequential methods are feasible for single time point studies that emphasize spatial correlation between structure and function but will result in an approximate doubling of the scan time for the same scan parameters when compared to a simultaneous approach. Although several truly simultaneous imaging approaches that remove this scan time increase have been proposed (20, 22–24), these techniques are not well suited for HP imaging studies due to the strict temporal (29) and spectral (30) imaging requirements required to capture the uptake and dynamics of metabolically active substrates in-vivo.

The present work introduces a method to acquire structural ^{1}H and functional ^{13}C spectroscopic MR data simultaneously for improved acquisition efficiency and correlation between datasets. To demonstrate the feasibility and flexibility of simultaneous multinuclear spectroscopic imaging of ^{1}H and HP ^{13}C, Cartesian and spiral pulse sequences were used with a spectral-spatial (SPSP) excitation. Single-band SPSP pulses allowed independent flip-angles for each chemical species, thus exciting only a single resonance at each TR and removing the need for spectral encoding regardless of the spectral complexity for each respective imaging channel (31). Simultaneously acquired ^{1}H and HP ^{13}C images are demonstrated to provide complementary information to better localize and visualize ^{13}C metabolic function in the context of ^{1}H anatomic structure.

Theory

Simultaneous Acquisition and Reconstruction

In our approach, we aim to excite and encode spins of differing nuclear gyromagnetic ratios (γ) with a single-band, spectral-spatial radio-frequency (RF) pulse followed by standard imaging gradients. As such, simultaneous techniques can be applied to any two or more nuclei assuming negligible spin-spin interaction between said nuclei. This work will specifically focus on the combination of ^{1}H and ^{13}C nuclei; in this case, the large γ difference results in J-coupling as the only prominent potential direct interaction (32). This J-coupling effect is mitigated by commonly used ^{13}C labels which aim to isolate hyperpolarized nuclei. For example, in the case of [1-^{13}C]pyruvate the enriched carbon is quaternary and isolated from ^{1}H nuclei, resulting in minimal J_{CH} coupling.

The remaining consequences of differing γ relate to spatial encoding, namely slice selection and k-space coverage. Unlike conventional slice-selective approaches, spectral-spatial pulses enable excitation that is both spatially and spectrally selective (33). Similar to a conventional broadband excitation, the spatial response (i.e. slice thickness) is determined by the bandwidth of the individual subpulses and is a function of both the oscillating slice selection gradient played during the RF pulse and the nuclear gyromagnetic ratio (34). Given equivalent slice-selection parameters, the carbon slice will therefore have four times the thickness ($\gamma^{13}\text{C} \approx ¼\ \gamma^{1}\text{H}$) of the proton slice. Since excitation can be performed independently on both channels, different RF pulses of the same duration could be used to mitigate this difference, potentially with tailored subpulses and flip angle for each nucleus of interest. For demonstrating feasibility in this work, the RF pulse was identical on both channels, resulting in a slice thickness for ^{13}C that was four times that of ^{1}H in order to

increase SNR. Unlike the spatial response, the spectral response is dependent only on the envelope and duration of the SPSP pulse and is the same spectral width for all nuclei being imaged.

The in-plane resolution and field-of-view (FOV) are also influenced by γ, which directly affects the spatial frequency. This dependence on the gyromagnetic ratio modulates the k-space trajectory (Fig. 1), resulting in a sampling pattern for ^{13}C that extends to only $\gamma^{13}C/\gamma^{1}H \approx ¼$ of k_{max} of the ^{1}H nucleus. Because the same gradient and sampling bandwidth is necessarily used for spatial encoding (Fig. 1A), the carbon nucleus spatial frequency sampling is four times more dense, leading to a four times larger FOV with four times lower resolution relative to ^{1}H sampling (Fig. 1B,C). A similar difference in sample interval and FOV is observed for the spiral trajectories implemented (not shown). Fortuitously, this fourfold reduction in resolution is advantageous in practice as HP metabolic imaging of ^{13}C-labelled metabolites can only support relatively large voxels due to the low concentration of the HP ^{13}C label in-vivo. This difference in FOV and resolution is easily accounted for during image reconstruction by scaling the k-space trajectory or during post-processing by interpolation in image-space.

Methods

MR Hardware Adaptations and Polarization

All experiments were performed on a horizontal bore 4.7T small animal scanner (Agilent, Palo Alto, CA) equipped with high performance gradients (400mT/m gradient strength, 2580T/m/s slew-rate). A commercial dual-tuned $^{1}H/^{13}C$ volume coil (Doty Scientific, Columbia, SC) was used for all experiments.

Simultaneous acquisition was enabled by performing a dual-channel gradient-spoiled GRE acquisition, with the transmission and demodulation frequencies independently set for ^{1}H and ^{13}C. Due to the scanner configuration, this was performed by adapting the decoupling functionality of the low-band amplifier to perform the ^{13}C excitation while simultaneously exciting ^{1}H nuclei with the high-band amplifier (Fig. 2). Because signal reception was performed with two separate amplifier channels, each nucleus was demodulated by the appropriate local oscillator frequency in hardware. Specifically, in the VNMRJ software, the RF pulse is set up to transmit on both frequencies simultaneously, similar to a decoupling pulse in NMR. Multiple receive coils are configured - in this case one for each nucleus - as for a parallel imaging experiment (Supplementary Table 1). In hardware, the preamplifier for ^{13}C is configured as if it is the 2^{nd} channel in a parallel imaging experiment. This means that the control cables are swapped such that the scanner is receiving ^{1}H data from the first channel and ^{13}C data from the second (Supplementary Figure 1). This is achieved by using the local oscillator line from the low-band transmitter (set at the ‘demodulation’ frequency of ^{13}C) and connecting it to the 2^{nd} preamplifier. In this way, each channel is demodulated at the preamplifier to 80MHz (as is standard on this system), and all remaining processing and saving of data are the standard settings for a ^{1}H scan with the prescribed parameters.

For polarization, 30μL aliquots of [1-^{13}C]pyruvic acid and 15mM trityl radical (OX63, GE Healthcare) were prepared and inserted into a Hypersense polarizer (Tubney Woods,

Abingdon, Oxfordshire, UK), cooled to 1.4K and irradiated with ~94GHz microwaves for approximately one hour. Samples were subsequently dissoluted with 4mL of 100mM NaOH/Tris and 250mg/L EDTA, resulting in a [1-^{13}C]pyruvate concentration of 100mM at physiologic temperature and pH. The polarized [1-^{13}C]pyruvate was drawn off and 10μL/g was rapidly injected via tail-vein cannulation. Animal temperature was maintained at 36.5 ± 0.5°C using a rectal probe coupled with a hot air blower for the duration of the experiment. All animal experiments were approved by IACUC and were performed according to protocol guidelines.

Phantom Experiments

To validate and test the efficacy of simultaneous SPSP excitation, a phantom consisting of three vials, one containing silicon oil with chemical shift $\Delta f(^1\text{H}) = -960$Hz; a second with ^{13}C urea dissolved in H_2O (7.7M; $\Delta f(^1\text{H}) = \Delta f(^{13}\text{C}) = 0$Hz), and a third with neat [1-^{13}C]acetic acid (17.4M; $\Delta f(^1\text{H}) = -530$Hz, $\Delta f(^{13}\text{C}) = 719$Hz) was used. The 15ms SPSP excitation was designed for independent excitation of [1-^{13}C]pyruvate and metabolites at 4.7T, resulting in a passband FWHM of 140Hz and stopband width of 1400Hz. These values were chosen to minimize stopband excitation of pyruvate-hydrate and bicarbonate when lactate was excited. Two sets of simultaneous ^{13}C and ^{1}H Cartesian gradient spoiled GRE images (TR/TE = 16.9/8.5ms, spectral width (SW) = 100kHz, 1.28ms readout, 128×128 matrix) were acquired with independent ^{1}H and ^{13}C excitation frequency offsets. Multinuclear image sets of water and ^{13}C urea were simultaneously acquired, followed by the ^{1}H and [1-^{13}C]acetic acid resonances. Data were reconstructed with a 2D Fourier transform, with the central 32 × 32 region of the ^{13}C images cropped and zero filled by a factor of 4 to match the ^{1}H resolution and FOV.

In-Vivo Experiments

For in-vivo experiments, two healthy ICR mice (one for each experiment) were fasted for 12 hours prior to imaging. Mice were anesthetized using 1.5% isoflurane and respiration was monitored using a respiratory pad in order to ensure a stable anesthetization (Small Animal Instruments, Stony Brook, NY).

Cartesian and spiral gradient spoiled GRE pulse sequences were modified to enable simultaneous acquisition of ^{1}H and ^{13}C species. ^{1}H data were acquired with a 0.5×0.5mm^2 in-plane resolution and a slice-thickness of 2.5mm, resulting in 2×2mm^2 in-plane resolution and a slice thickness of 10mm for ^{13}C metabolites. To demonstrate multinuclear and multispectral capabilities, two pairs of resonances were acquired per nucleus in sequential images: multinuclear image sets of [1-^{13}C]pyruvate and water were simultaneously acquired, followed immediately by simultaneous acquisition of [1-^{13}C]lactate and fat. Proton images were excited with a flip-angle of 15° while ^{13}C metabolites were excited with independent flip-angles (30° for [1-^{13}C]lactate, and 10° for [1-^{13}C]pyruvate) to more efficiently use the spin polarization over the duration of the experiment.

For the in-vivo Cartesian experiment, data were acquired with TR/TE = 16.9/8.5ms, SW = 10kHz, 6.4ms readout, and a 128×128 matrix size. In order to further conserve the ^{13}C polarization, the ^{13}C channel was excited only every 4th phase encode of the ^{1}H acquisition.

This maintains the same FOV (in the phase encoding direction) for both nuclei while mitigating ^{13}C polarization loss due to RF excitation, at the expense of four-fold longer total scan time. Data were reconstructed as described above and the ^{1}H images were used to localize and provide an anatomical reference for ^{13}C metabolite maps. In this experiment only one time point was acquired, corresponding to the peak lactate signal occurring 20s after the start of injection to emphasize applications requiring higher spatial localization of ^{13}C function to ^{1}H structure.

For the in-vivo spiral experiment, dynamic data were emphasized. Dynamic data were acquired with a fully-sampled single-shot trajectory (35), with a readout duration of 18.25ms. A 1D spectrum (5° flip-angle, 10kHz SW, 4096 complex points) was acquired at each timeframe to determine the relative frequencies of [1-^{13}C]pyruvate and downstream metabolites. Data acquisition began prior to injection, with a five second delay between timeframes to allow for metabolism to occur. In a separate post-scan step, the k-space trajectory was measured on the ^{1}H channel using a thin slice excitation method (36).

For analysis, spectra were multiplied with a 20Hz exponential filter prior to being Fourier transformed and phased. Spiral data were frequency demodulated based on the frequency difference between the transmitter frequency and apparent chemical shift from the acquired spectra to account for a global receiver offset. Data were then gridded and Fourier transformed to create metabolite maps for each species of interest. To account for the difference in gyromagnetic ratios, the k-space trajectory was scaled by a factor of ¼ prior to ^{13}C gridding to yield final images with equivalent FOVs for both nuclei. Metabolite time courses and lactate-to-pyruvate area under the curve (AUC) ratios (37) were obtained from imaging data based on kidney ROIs derived from the simultaneously acquired water data. To assess the degree of inter-scan bulk motion, the cross-correlation was calculated between the initial and subsequent ^{1}H images from each timeframe.

Results

Images from simultaneous SPSP excitation in a multinuclear phantom can be seen in Fig. 3. Comparing Fig. 3A with Fig. 3B and 3C illustrates the ability of simultaneous SPSP excitation to individually excite and reconstruct images of vials containing ^{1}H and ^{13}C chemical species separately. Note that for this data the difference in γ leads to a four-fold thicker ^{13}C slice (10mm as compared to 2.5mm), offsetting the reduced SNR expected for the lower receptivity of ^{13}C nuclei at Boltzmann equilibrium. Experimental results support the ability to achieve strong off-resonance suppression without visible cross-talk between the two nuclei or resonances, enabling robust simultaneous imaging of specific chemical species.

Based on the phantom experiments, the method was extended to preliminary in-vivo studies of renal metabolism in a healthy mouse model to assess feasibility. Fat and water images (Fig. 4A, B) acquired at 0.5mm in-plane resolution with a Cartesian acquisition show excellent separation of the renal cortex from the adipose tissue surrounding the kidney. Signal is attenuated in the ventral region of the proton images due to field inhomogeneities arising from the respiratory pad used for animal monitoring. Metabolite maps of

[1-^{13}C]lactate and [1-^{13}C]pyruvate (Fig. 4C, D) agree with the expected underlying anatomy obtained from the water images. No dynamic images were acquired in this experiment in favor of a single time point image acquired at the time of peak [1-^{13}C]lactate signal.

Dynamic images of renal metabolism of [1-^{13}C]pyruvate and [1-^{13}C]lactate acquired with a spiral acquisition every 5s can be seen in Fig. 5. Similar to the simultaneously acquired Cartesian data, images of [1-^{13}C]pyruvate delivered via tail vein intravenous injection are dominated by the vasculature while images of lactate indicate strong metabolism in the kidneys. Dynamic ^{1}H data show kidney motion during the experiment, likely due to respiratory motion between time frames. This is most visible in the 4th timeframe (Fig. 6), and is readily apparent when the normalized cross-correlation between simultaneously acquired water time frames is measured. It is feasible to use the ^{1}H image to either guide placement of the ROIs for quantitative measures or to discard motion-corrupted frames from the analysis. In this case, the lactate-to-pyruvate AUC ratio was calculated from an ROI shifted to account for the motion. The motion compensated results for the AUC ratio differed by nearly 15% (0.713 vs. 0.819 for the static and dynamic ROIs, respectively). Note that the simultaneously acquired ^{13}C data are distorted as a result of the motion detected on the high-resolution structural ^{1}H image and this allows the analysis to be adapted accordingly.

Discussion

This study demonstrates the feasibility of a simultaneous ^{1}H/^{13}C acquisition with SPSP excitation using both Cartesian and spiral pulse sequences. Two test cases were demonstrated, emphasizing improved structure-function association and dynamic motion tracking for imaging renal metabolism, respectively. This method adapts the decoupling channel of our commercial small animal MRI scanner to enable independently tunable broadband and proton transceiver channels that are integrated within standard system hardware and software. This approach for simultaneous imaging requires hardware that may not be initially available on all vendor platforms, but was available on our Agilent small animal scanner with minor hardware (<5 minute setup) and pulse sequence modifications to accommodate simultaneous SPSP excitation and reception.

The Cartesian data are presented as a proof of concept for the combination of SPSP imaging with simultaneous multinuclear excitation, as well as to demonstrate the flexibility of the proposed simultaneous imaging method. In the in-vivo experiments, every 4th phase encode was acquired on the ^{13}C channel to minimize RF deposition and match the ^{1}H FOV in the phase encode direction. The scan time is therefore increased fourfold when compared to an acquisition that only acquires ^{13}C data directly but with the potential advantage of improved spatial-temporal correlation of structure and function. Despite the scan time inefficiencies compared to single-shot methods (e.g. spiral), there are benefits to a conventional trajectory in circumstances where spatial resolution is emphasized over temporal resolution. This is a consequence of the Cartesian acquisition's relative robustness to off-resonance and trajectory errors. In such interleaved acquisition scenarios the potential exists for a mixture of thermal T_1 recovery for ^{1}H and hyperpolarized non-equilibrium T_1 decay for the hyperpolarized ^{13}C species. An interleaved Cartesian approach would enable different view

orders for both nuclei, and extended TR intervals for the ^{1}H nucleus may make sense in some applications to allow for T_1 recovery between higher frequency ^{13}C excitations, especially in circumstances where higher resolution ^{1}H data are of interest. Since ^{1}H imaging can support much higher resolutions, the total imaging time in such a scenario will likely more than double but with positive benefits in terms of SNR and resolution.

The feasibility of truly simultaneous imaging, i.e. for every single TR, was also shown for a non-Cartesian spiral acquisition specifically for a dynamic imaging application. Whereas Cartesian acquisitions are more robust to off-resonance effects, they are RF inefficient and have a coarser temporal resolution when used for dynamic imaging. Moreover, coupling SPSP excitation with a non-Cartesian readout removes the need for spectral encoding, greatly simplifying acquisition and reconstruction while enabling the use of automatic off-resonance correction algorithms (38–41) that are incompatible when multiple chemical species are excited. While the spiral ^{1}H data acquired in a single-shot is unable to provide the structural detail of a high-resolution Cartesian image, it can be used to track bulk motion using mutual information or cross-correlation methods to quantify misregistration and retrospectively correct (22) or allow for the omission of corrupted timeframes. Due to the coarse spatial resolution typically used in HP ^{13}C experiments, motion between scans can appear as aberrant metabolism outside the organ of interest, potentially obfuscating kinetic measures. Respiratory motion of the kidney is well documented in human patients (42–44) and is likely to be a concern even in small animal studies. By also acquiring a ^{1}H image concurrently, the ROI for kinetic measures of metabolism can be updated at each timeframe and kinetic data can be corrected for inter-scan motion. Furthermore, employing a single-shot readout as in the spiral acquisition minimizes potential artifacts arising from motion between multi-shot encodings.

One limitation of this approach is that a simultaneous acquisition requires specialized hardware and may require tradeoffs between the optimal imaging parameters for both nuclei. Any implementation would require, at minimum, a dual-tuned, multinuclear coil or a standalone ^{13}C coil if a ^{1}H body coil is present, along with separate ^{1}H and x-nuclei/broadband RF amplifiers. While construction of dual-tuned coils is relatively straightforward for well-separated frequencies, their construction becomes more difficult for nuclei pairs with similar Larmor frequencies, such as $^{1}H/^{19}F$ (45). Differences in T_2^* between the two nuclei will place limitations on the optimal readout duration before blurring becomes apparent, while the difference in γ will modulate the FOV and reduce spatial resolution for the lower γ nucleus. In practice, the fourfold difference between the ^{13}C and ^{1}H gyromagnetic ratio is fortuitous as it results in spatial or temporal resolution tradeoffs that are sufficient for visualizing both nuclei on the time scale of dynamic metabolism. Nevertheless, the difference in γ between other nuclei pairs may be suboptimal for a given application. In this case, an interleaved excitation scheme (25) or post-processing techniques may be required to generate images with the desired resolution for both nuclei.

A second limitation is the small sample size in this study. The focus of the present work is necessarily on demonstrating the technical feasibility and the consequences of using a simultaneous approach to $^{13}C/^{1}H$ acquisition. Given the implementation on a small animal imaging system, additional hardware flexibility is gained compared to clinical MRI systems,

enabling a truly simultaneous acquisition. Additional studies are needed to rigorously validate the proposed applications to improve image quality for structure-function association and dynamic imaging.

While this work focuses on imaging of ^{1}H structure and ^{13}C metabolism, it is readily amenable to other structure-function applications in low signal nuclei like ^{23}Na, ^{31}P, or ^{19}F, or methodologies where data acquisition in a short period of time is paramount such as HP studies of ^{3}He or ^{129}Xe. The method is straightforward, easy to implement, and provides similar imaging capabilities for all nuclei that are being imaged. Other potential advantages that were not explored in this work include real-time field mapping (46) or deformable registration strategies. The flexibility of the acquisition strategy allows for a variety of possible acquisitions or correction methods that could improve the quality of multinuclear structure-function imaging. This technique can be naturally extended to MRI acquisition strategies such as parallel imaging and compressed sensing. It is anticipated that the method can be combined with most pulse sequences, and is compatible with more than two nuclei as long as the appropriate scanner hardware adaptations are available.

Conclusion

This work demonstrates a method for simultaneously acquiring multinuclear spectroscopic data during a single scan. Both Cartesian and spiral implementations are shown, and the flexibility of SPSP RF pulses is demonstrated by simultaneously acquiring specific resonances on both the ^{1}H and ^{13}C channels. By virtue of the simultaneous acquisition, structural ^{1}H data are spatially and temporally correlated with the functional ^{13}C data allowing for potentially improved quantitative analysis with minimal to no increase in scan time.

Supplementary Material

Refer to Web version on PubMed Central for supplementary material.

Acknowledgments

Funding Acknowledgements: The authors would like to thank the University of Wisconsin Alzheimer's Disease Research Center NIH P50AG033514 and the Carbone Comprehensive Cancer Center (UWCCC) NIH/NCI P30 CA014520 for the funds to complete this project. This work is also supported in part by the Medical Physics NCI Radiological Sciences Training Grant NIH/NCI T32 CA009206, GE Healthcare, and the University of Wisconsin Graduate School.

Abbreviations

DNP	dynamic nuclear polarization
SPSP	spectral-spatial
FOV	field of view
HP	hyperpolarized
AUC	area under the curve

NaOH	sodium hydroxide
TRIS	tris(hydroxymethyl)aminomethane
SW	spectral width

References

1. Ardenkjær-Larsen JH, Fridlund B, Gram A, Hansson G, Hansson L, Lerche MH, Servin R, Thaning M, Golman K. Increase in signal-to-noise ratio of >10,000 times in liquid-state NMR. Proc Natl Acad Sci USA. 2003; 100(18):10158–10163. [PubMed: 12930897]
2. Golman K, Ardenkjær-Larsen JH, Petersson JS, Månsson S, Leunbach I. Molecular imaging with endogenous substances. Proc Natl Acad Sci USA. 2003; 100(18):10435–10439. [PubMed: 12930896]
3. Svensson J, Månsson S, Johansson E, Petersson JS, Olsson LE. Hyperpolarized 13C MR angiography using trueFISP. Magnetic Resonance in Medicine. 2003; 50(2):256–262. [PubMed: 12876701]
4. Day SE, Kettunen MI, Gallagher FA, Hu DE, Lerche M, Wolber J, Golman K, Ardenkjaer-Larsen JH, Brindle KM. Detecting tumor response to treatment using hyperpolarized 13C magnetic resonance imaging and spectroscopy. Nat Med. 2007; 13(11):1382–1387. [PubMed: 17965722]
5. Day SE, Kettunen MI, Cherukuri MK, Mitchell JB, Lizak MJ, Morris HD, Matsumoto S, Koretsky AP, Brindle KM. Detecting response of rat C6 glioma tumors to radiotherapy using hyperpolarized [1-13C]pyruvate and 13C magnetic resonance spectroscopic imaging. Magnetic Resonance in Medicine. 2011; 65(2):557–563. [PubMed: 21264939]
6. Albers MJ, Bok R, Chen AP, Cunningham CH, Zierhut ML, Zhang VY, Kohler SJ, Tropp J, Hurd RE, Yen Y-F, Nelson SJ, Vigneron DB, Kurhanewicz J. Hyperpolarized 13C Lactate, Pyruvate, and Alanine: Noninvasive Biomarkers for Prostate Cancer Detection and Grading. Cancer Res. 2008; 68(20):8607–8615. [PubMed: 18922937]
7. Zierhut ML, Yen Y-F, Chen AP, Bok R, Albers MJ, Zhang V, Tropp J, Park I, Vigneron DB, Kurhanewicz J, Hurd RE, Nelson SJ. Kinetic modeling of hyperpolarized 13C1-pyruvate metabolism in normal rats and TRAMP mice. Journal of Magnetic Resonance. 2010; 202(1):85–92. [PubMed: 19884027]
8. Smith M, Peterson E, Gordon J, Niles D, Rowland I, Kurpad K, Fain S. In-vivo imaging and spectroscopy of dynamic metabolism using simultaneous 13C and 1H MRI. Biomedical Engineering, IEEE Transactions on. 2011; PP(99):45–49.
9. Mayer D, Yen Y-F, Tropp J, Pfefferbaum A, Hurd RE, Spielman DM. Application of subsecond spiral chemical shift imaging to real-time multislice metabolic imaging of the rat in vivo after injection of hyperpolarized 13C1-pyruvate. Magnetic Resonance in Medicine. 2009; 62(3):557–564. [PubMed: 19585607]
10. Witney TH, Kettunen MI, Hu De, Gallagher FA, Bohndiek SE, Napolitano R, Brindle KM. Detecting treatment response in a model of human breast adenocarcinoma using hyperpolarised [1-13C] pyruvate and [1,4-13C2] fumarate. Br J Cancer. 2010; 103(9):1400–1406. [PubMed: 20924379]
11. Darpolor MM, Yen Y-F, Chua M-S, Xing L, Clarke-Katzenberg RH, Shi W, Mayer D, Josan S, Hurd RE, Pfefferbaum A, Senadheera L, So S, Hofmann LV, Glazer GM, Spielman DM. In vivo MRSI of hyperpolarized [1-13C]pyruvate metabolism in rat hepatocellular carcinoma. NMR Biomed. 2010:506–513. [PubMed: 21674652]
12. Chen AP, Hurd RE, Schroeder MA, Lau AZ, Gu Y-p, Lam WW, Barry J, Tropp J, Cunningham CH. Simultaneous investigation of cardiac pyruvate dehydrogenase flux, Krebs cycle metabolism and pH, using hyperpolarized [1,2-13C2]pyruvate in vivo. NMR in Biomedicine. 2012; 25(2): 305–311. [PubMed: 21774012]
13. Hurd RE, Yen Y-F, Mayer D, Chen A, Wilson D, Kohler S, Bok R, Vigneron D, Kurhanewicz J, Tropp J, Spielman D, Pfefferbaum A. Metabolic imaging in the anesthetized rat brain using

hyperpolarized [1-13C] pyruvate and [1-13C] ethyl pyruvate. Magnetic Resonance in Medicine. 2010; 63(5):1137–1143. [PubMed: 20432284]

14. Gallagher FA, Kettunen MI, Brindle KM. Imaging pH with hyperpolarized 13C. NMR in Biomedicine. 2011; 24(8):1006–1015. [PubMed: 21812047]
15. Gallagher FA, Kettunen MI, Day SE, Hu D-e, Karlsson M, Gisselsson A, Lerche MH, Brindle KM. Detection of tumor glutamate metabolism in vivo using 13C magnetic resonance spectroscopy and hyperpolarized [1-13C]glutamate. Magnetic Resonance in Medicine. 2011; 66(1):18–23. [PubMed: 21695718]
16. Gabellieri C, Leach MO, Eykyn TR. Modulating the relaxivity of hyperpolarized substrates with gadolinium contrast agents. Contrast Media Mol Imaging. 2009; 4(3):143–147. [PubMed: 19330792]
17. Merritt ME, Harrison C, Kovacs Z, Kshirsagar P, Malloy CR, Sherry AD. Hyperpolarized 89Y Offers the Potential of Direct Imaging of Metal Ions in Biological Systems by Magnetic Resonance. Journal of the American Chemical Society. 2007; 129(43):12942–12943. [PubMed: 17927188]
18. Jindal AK, Merritt ME, Suh EH, Malloy CR, Sherry AD, Kovács Zn. Hyperpolarized 89Y Complexes as pH Sensitive NMR Probes. Journal of the American Chemical Society. 2010; 132(6):1784–1785. [PubMed: 20102196]
19. Lumata L, Merritt ME, Hashami Z, Ratnakar SJ, Kovacs Z. Production and NMR Characterization of Hyperpolarized 107,109Ag Complexes. Angewandte Chemie International Edition. 2012; 51(2):525–527.
20. Moore GJ, Hrovat MI, González RG. Simultaneous multinuclear magnetic resonance imaging and spectroscopy. Magnetic Resonance in Medicine. 1991; 19(1):105–112. [PubMed: 2046525]
21. van Sluis R, Yongbi NM, Payne GS, Leach MO. Simultaneous localized 1H STEAM/31P ISIS spectroscopy in Vivo. Magnetic Resonance in Medicine. 1996; 35(4):465–470. [PubMed: 8992195]
22. Keupp J, Rahmer J, Grässlin I, Mazurkewitz PC, Schaeffter T, Lanza GM, Wickline SA, Caruthers SD. Simultaneous dual-nuclei imaging for motion corrected detection and quantification of 19F imaging agents. Magnetic Resonance in Medicine. 2011; 66(4):1116–1122. [PubMed: 21394779]
23. Wild JM, Marshall H, Xu X, Norquay G, Parnell SR, Clemence M, Griffiths PD, Parra-Robles J. Simultaneous Imaging of Lung Structure and Function with Triple-Nuclear Hybrid MR Imaging. Radiology. 2013; 267(1):251–255. [PubMed: 23264344]
24. Lee SW, Hilal SK, Cho ZH. A multinuclear magnetic resonance imaging technique-simultaneous proton and sodium imaging. Magnetic Resonance Imaging. 1986; 4(4):343–350. [PubMed: 2823046]
25. Gonen O, Murphyboesch J, Srinivasan R, Hu JN, Jiang H, Stoyanova R, Brown TR. Simultaneous and Interleaved Multinuclear Chemical-Shift Imaging, a Method for Concurrent, Localized Spectroscopy. Journal of Magnetic Resonance, Series B. 1994; 104(1):26–33. [PubMed: 8025812]
26. Wild JM, Ajraoui S, Deppe MH, Parnell SR, Marshall H, Parra-Robles J, Ireland RH. Synchronous acquisition of hyperpolarised 3He and 1H MR images of the lungs – maximising mutual anatomical and functional information. NMR in Biomedicine. 2011; 24(2):130–134. [PubMed: 20821726]
27. Kurhanewicz J, Vigneron DB, Brindle K, Chekmenev EY, Comment A, Cunningham CH, DeBerardinis RJ, Green GG, Leach MO, Rajan SS, Rizi RR, Ross BD, Warren WS, Malloy CR. Analysis of Cancer Metabolism by Imaging Hyperpolarized Nuclei: Prospects for Translation to Clinical Research. Neoplasia. 2011; 13(2):81–97. [PubMed: 21403835]
28. Gallagher FA, Kettunen MI, Brindle KM. Biomedical applications of hyperpolarized 13C magnetic resonance imaging. Progress in Nuclear Magnetic Resonance Spectroscopy. 2009; 55(4):285–295.
29. Xing Y, Reed GD, Pauly JM, Kerr AB, Larson PEZ. Optimal variable flip angle schemes for dynamic acquisition of exchanging hyperpolarized substrates. Journal of Magnetic Resonance. 2013; 234(0):75–81. [PubMed: 23845910]
30. Golman K, Zandt Rit, Lerche M, Pehrson R, Ardenkjaer-Larsen JH. Metabolic Imaging by Hyperpolarized 13C Magnetic Resonance Imaging for In vivo Tumor Diagnosis. Cancer Research. 2006; 66(22):10855–10860. [PubMed: 17108122]

31. Cunningham CH, Chen AP, Lustig M, Hargreaves BA, Lupo J, Xu D, Kurhanewicz J, Hurd RE, Pauly JM, Nelson SJ, Vigneron DB. Pulse sequence for dynamic volumetric imaging of hyperpolarized metabolic products. Journal of Magnetic Resonance. 2008; 193(1):139–146. [PubMed: 18424203]
32. Chen AP, Tropp J, Hurd RE, Criekinge MV, Carvajal LG, Xu D, Kurhanewicz J, Vigneron DB. In vivo hyperpolarized 13C MR spectroscopic imaging with 1H decoupling. Journal of Magnetic Resonance. 2009; 197(1):100–106. [PubMed: 19112035]
33. Meyer CH, Pauly JM, Macovskiand A, Nishimura DG. Simultaneous spatial and spectral selective excitation. Magnetic Resonance in Medicine. 1990; 15(2):287–304. [PubMed: 2392053]
34. Schulte RF, Wiesinger F. Direct design of 2D RF pulses using matrix inversion. Journal of Magnetic Resonance. 2013; 235(0):115–120. [PubMed: 24013595]
35. Glover GH. Simple analytic spiral K-space algorithm. Magnetic Resonance in Medicine. 1999; 42(2):412–415. [PubMed: 10440968]
36. Duyn JH, Yang Y, Frank JA, van der Veen JW. Simple Correction Method for k-Space Trajectory Deviations in MRI. Journal of Magnetic Resonance. 1998; 132(1):150–153. [PubMed: 9615415]
37. Hill DK, Orton MR, Mariotti E, Boult JKR, Panek R, Jafar M, Parkes HG, Jamin Y, Miniotis MF, Al-Saffar NMS, Beloueche-Babari M, Robinson SP, Leach MO, Chung Y-L, Eykyn TR. Model Free Approach to Kinetic Analysis of Real-Time Hyperpolarized 13C Magnetic Resonance Spectroscopy Data. PLoS ONE. 2013; 8(9):e71996. [PubMed: 24023724]
38. Man L-C, Pauly JM, Macovski A. Improved automatic off-resonance correction without a field map in spiral imaging. Magnetic Resonance in Medicine. 1997; 37(6):906–913. [PubMed: 9178243]
39. Smith TB, Nayak KS. Automatic off-resonance correction in spiral imaging with piecewise linear autofocus. Magnetic Resonance in Medicine. 2012:82–90. [PubMed: 22457262]
40. Chen W, Meyer CH. Fast automatic linear off-resonance correction method for spiral imaging. Magnetic Resonance in Medicine. 2006; 56(2):457–462. [PubMed: 16810696]
41. Lau AZ, Chen AP, Ghugre NR, Ramanan V, Lam WW, Connelly KA, Wright GA, Cunningham CH. Rapid multislice imaging of hyperpolarized 13C pyruvate and bicarbonate in the heart. Magnetic Resonance in Medicine. 2010; 64(5):1323–1331. [PubMed: 20574989]
42. Moerland MA, van den Bergh ACM, Bhagwandien R, Janssen WM, Bakker CJG, Lagendijk JJW, Battermann JJ. The influence of respiration induced motion of the kidneys on the accuracy of radiotherapy treatment planning, a magnetic resonance imaging study. Radiotherapy and Oncology. 1994; 30(2):150–154. [PubMed: 8184113]
43. Michoux N, Vallée JP, Pechère-Bertschi A, Montet X, Buehler L, Van Beers BE. Analysis of contrast-enhanced MR images to assess renal function. Magn Reson Mater Phy. 2006; 19(4):167–179.
44. Zöllner FG, Sance R, Rogelj P, Ledesma-Carbayo MJ, Rørvik J, Santos A, Lundervold A. Assessment of 3D DCE-MRI of the kidneys using non-rigid image registration and segmentation of voxel time courses. Computerized Medical Imaging and Graphics. 2009; 33(3):171–181. [PubMed: 19135861]
45. Hu S, Reimer JA, Bell AT. Single-input double-tuned circuit for double resonance nuclear magnetic resonance experiments. Review of Scientific Instruments. 1998; 69(2):477–478.
46. Gordon J, Niles D, Johnson K, Smith M, Kurpad K, Peterson E, Fain S. Simultaneous Imaging of 13C Metabolism and 1H Structure for Improved Co-Registration and Off-Resonance Correction. Proc Int Soc Magn Reson Med. 2013:3936.

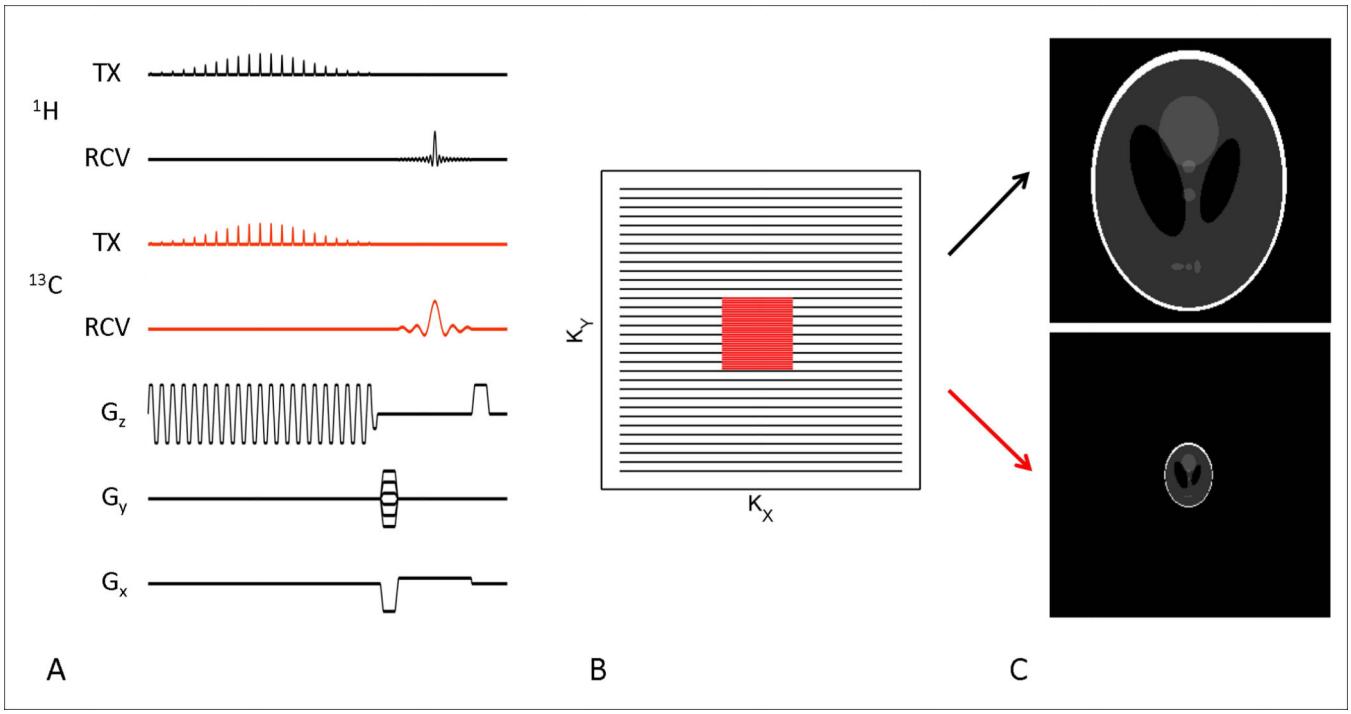

Figure 1.

The simultaneous pulse sequence (A) illustrates the design and playout for the concurrent Cartesian acquisition of ^{1}H and ^{13}C used in this work. The slice-thickness and k-space trajectory (B) is modulated by the γ of each nucleus, affecting both the resolution and FOV of the ^{13}C data (C). These differences can be readily corrected for combined structure-function by upsampling the image from the lower γ species.

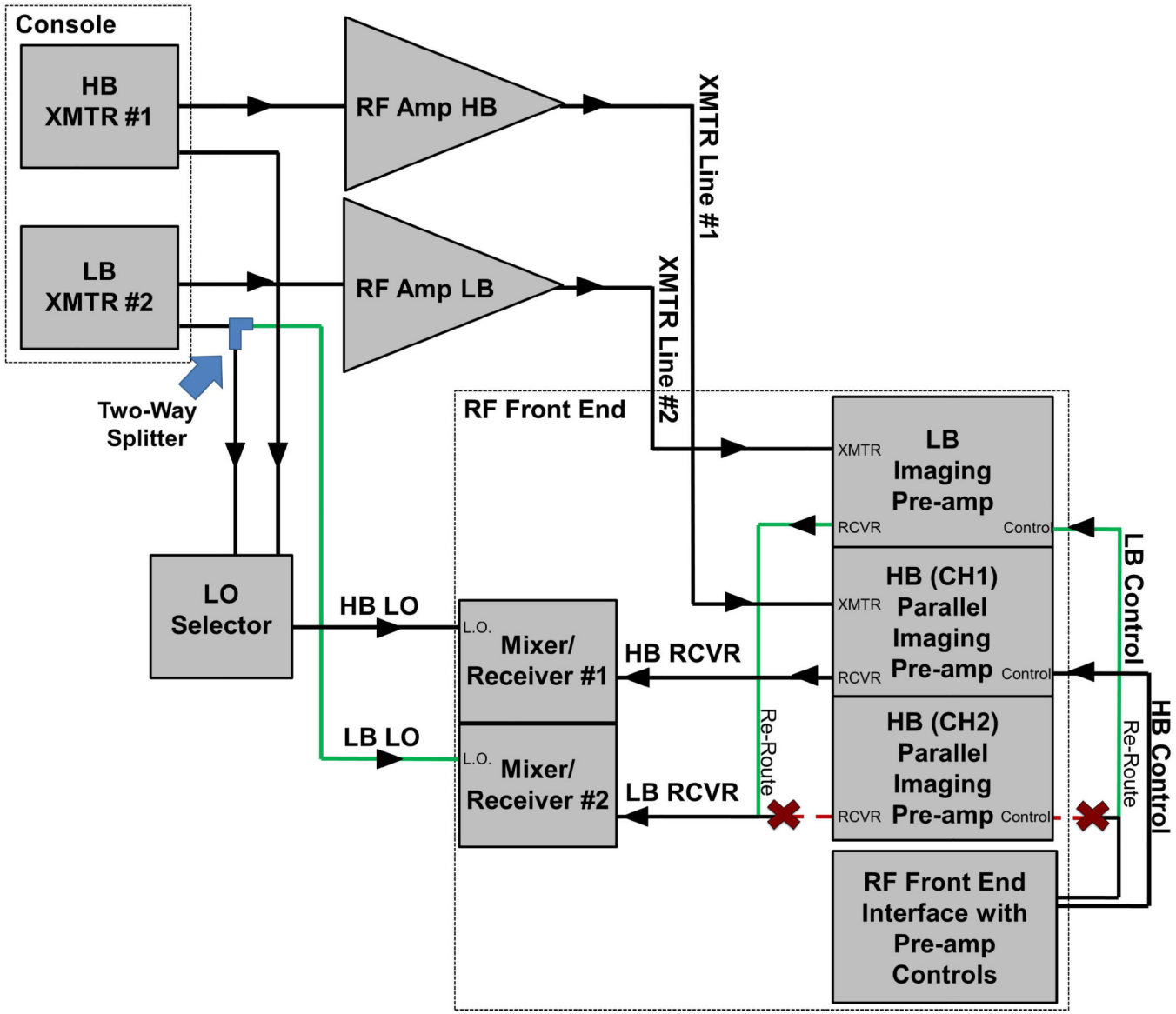

Figure 2.

Block diagram of hardware changes necessary for simultaneous acquisition. The low band (LB) local oscillator (LO) frequency is split from the LB transmitter (XMTR) board output and routed directly into the 2nd mixer/receiver dedicated to the LB frequency. The receiver (RCVR) and control lines for the 2nd high band (HB) parallel imaging pre-amp are re-routed and connected to the LB pre-amp.

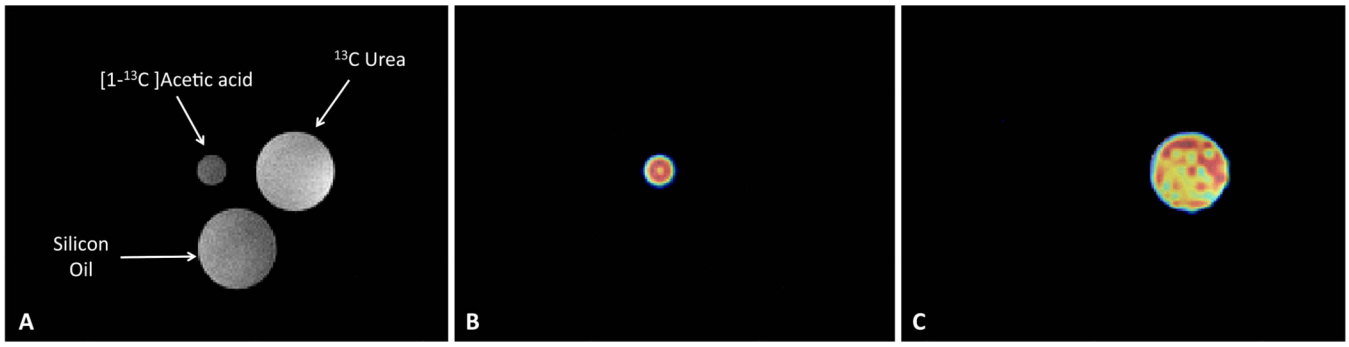

Figure 3.

Image experiments of the multispectral phantom (A) consisting of silicon oil, [1-^{13}C]acetic acid, and ^{13}C urea dissolved in H_2O. Independent control of ^{1}H and ^{13}C frequency offsets allows for selective excitation of both ^{1}H and ^{13}C species simultaneously (B: $\Delta f(^{1}H) = -530$Hz, $\Delta f(^{13}C) = 719$Hz; C: $\Delta f(^{1}H) = 0$Hz, $\Delta f(^{13}C) = 0$Hz). ^{1}H data is in grayscale, with ^{13}C data overlaid in color.

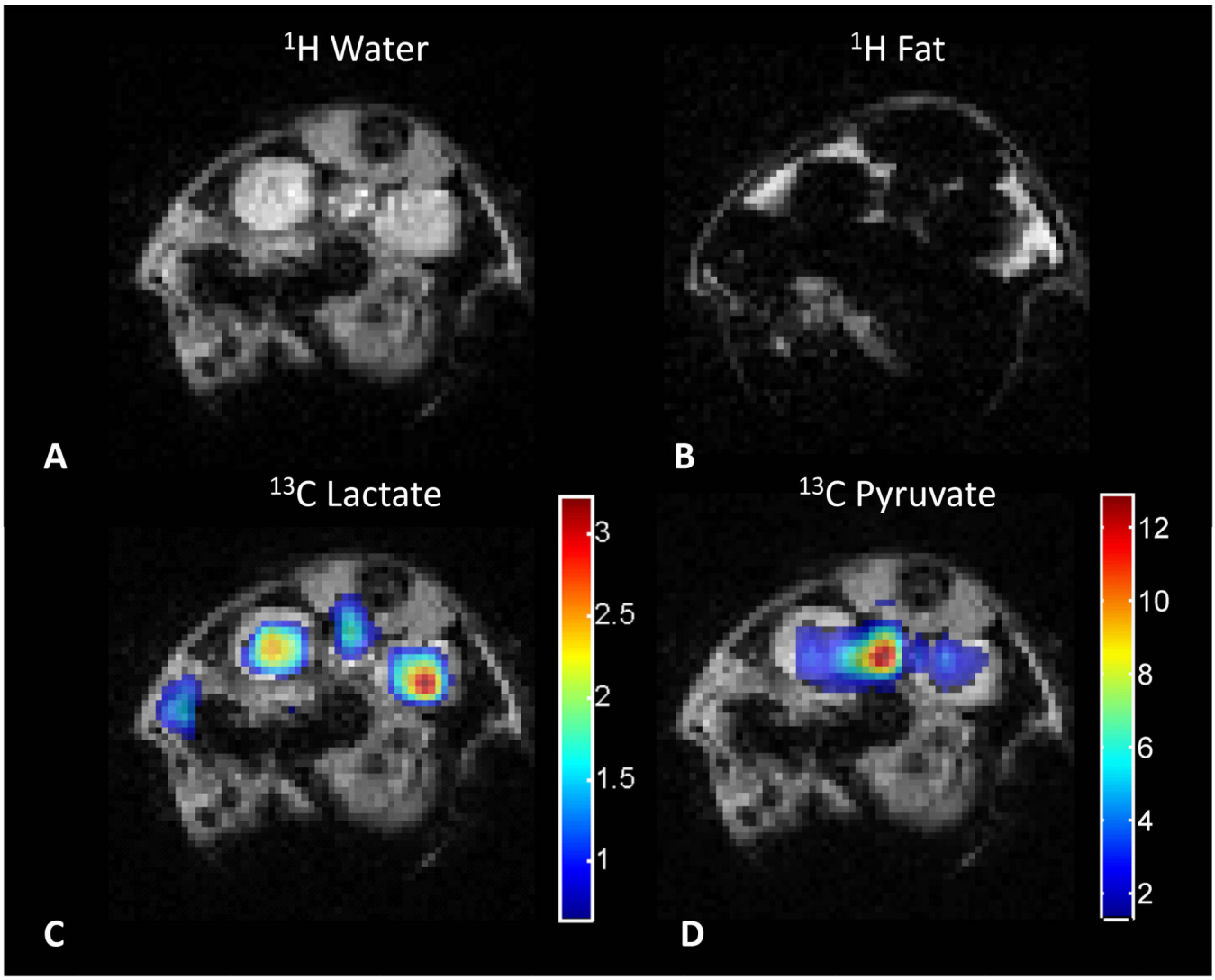

Figure 4.

Simultaneously acquired images of soft tissue anatomy (water and fat) and renal metabolism acquired with a SPSP excitation and gradient spoiled GRE Cartesian acquisition. Proton images show excellent spectral separation of water (A) and fat (B). Images of lactate (C) and pyruvate (D) agree well with the underlying anatomy from the simultaneously acquired water image. ^{13}C metabolite maps are in arbitrary units and were independently thresholded. Signal is attenuated in the ventral region of the ^{1}H images from the respiratory pad used for animal monitoring.

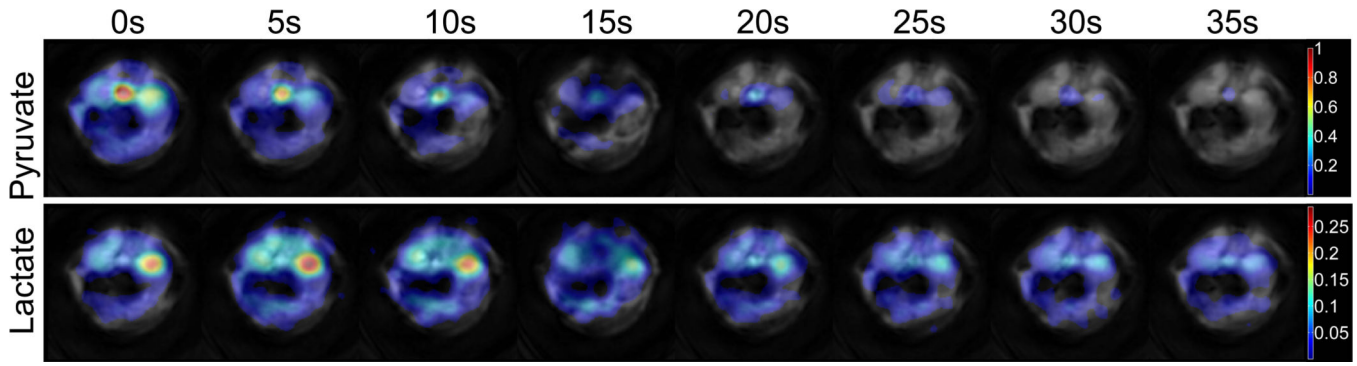

Figure 5.

Simultaneous images of renal metabolism (in units of normalized intensity) acquired with a SPSP excitation and a spiral acquisition. Both pyruvate and lactate metabolite maps agree with the underlying ^{1}H anatomy, even in the case of apparent motion induced distortion at 15s (frame 4). The timestamp is referenced to time from peak pyruvate signal.

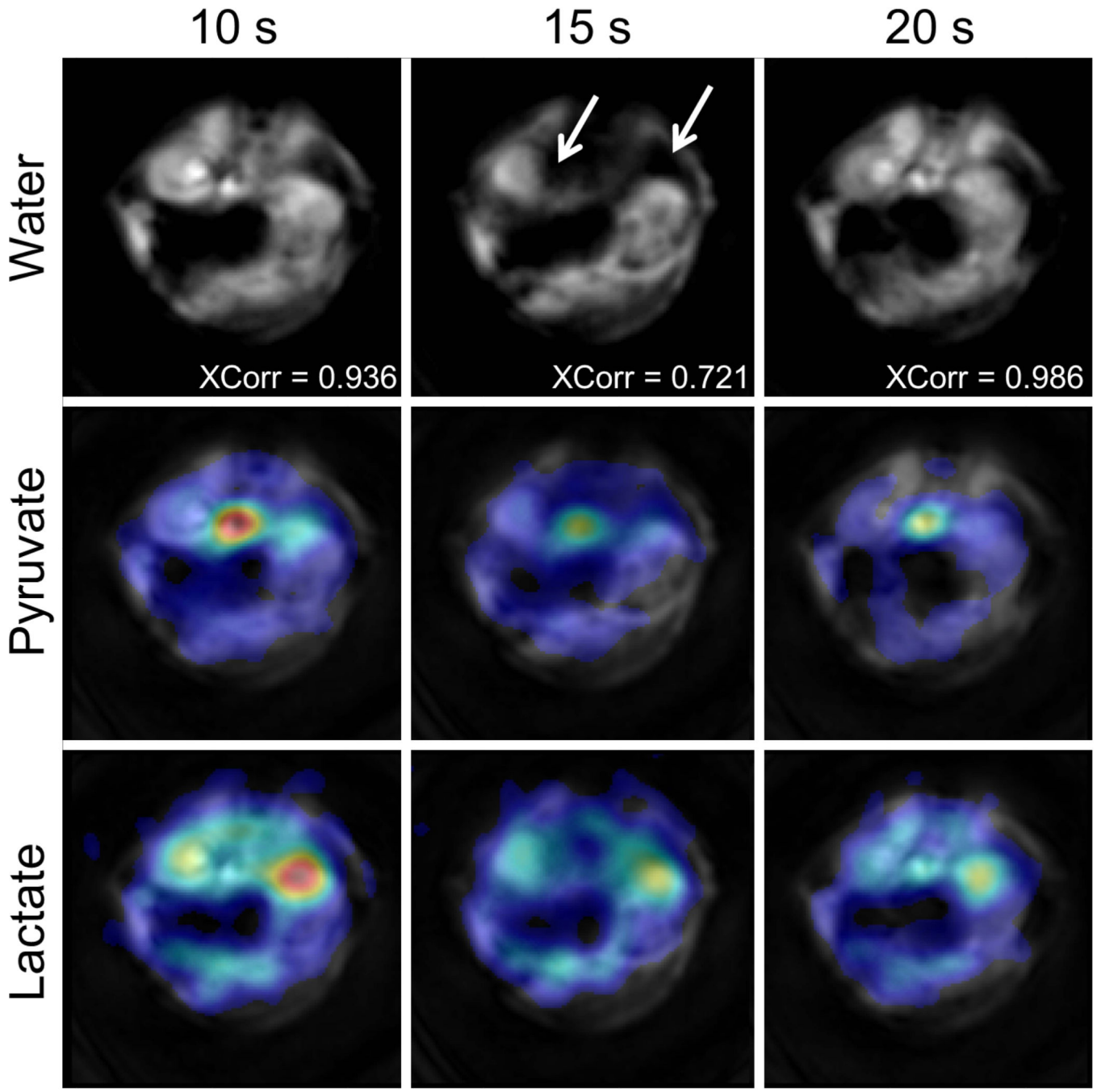

Figure 6.

Timeframes 3–5 from the simultaneous SPSP spiral acquisition. Frame 4 (15s) exhibits artifacts due to bulk/respiratory motion that are not present in adjacent timeframes. The normalized cross-correlation (XCorr) between water timeframes indicated in the lower right corner of the ^{1}H water images highlights this inter-scan motion and distortion.